Deconsolidation of thermoplastic prepreg tapes during rapid laser heating

Çelik, Ozan; Choudhary, Abhas; Peeters, Daniël; Teuwen, Julie; Dransfeld, Clemens

DOI
10.1016/j.compositesa.2021.106575

Publication date
2021

Document Version
Final published version

Published in
Composites Part A: Applied Science and Manufacturing

Composites: Part A 149 (2021) 106575

Contents lists available at ScienceDirect

Composites Part A

journal homepage: www.elsevier.com/locate/compositesa

Deconsolidation of thermoplastic prepreg tapes during rapid laser heating

Ozan Çelik *, Abhas Choudhary, Daniël Peeters, Julie Teuwen, Clemens Dransfeld

Aerospace Manufacturing Technologies, Faculty of Aerospace Engineering, Delft University of Technology, Kluyverweg 1, Delft 2629HS, the Netherlands

ARTICLE INFO

Keywords:
A. Polymer-matrix composites (PMCs)
B. Microstructures
D. Process monitoring
E. Automated fiber placement (AFP)

ABSTRACT

In this study, the effect of rapid laser heating, which is typical during laser-assisted fiber placement (LAFP), on the micro- and meso- structure of the thermoplastic tape was investigated. Thermoplastic tapes were heated above the melting temperature with different heated lengths (30 and 80 mm and heating times (0.2 and 0.8 s) in a dedicated experimental setup. In-situ and ex-situ characterization techniques were used to observe the differences between the micro- and meso- structure of the tape before and after heating. The experiments resulted in significant changes in the tape structure, namely increased out-of-plane deformation, waviness, arc-length width, roughness, thickness and volumetric void content. This study shows for the first time that a unique deconsolidation behavior takes place during the heating phase of LAFP: the deconsolidation mechanisms are exacerbated by the non-uniform temperature at the tape surface, which is caused by roughness increase and waviness formation.

1. Introduction

Strict limitations on CO_2 emissions pushes the aerospace and automotive industry to produce more efficient vehicles with alternative energy sources. This makes weight reduction one of the primary goals for these industries. High performance composite materials provide a solution to the weight reduction problem owing to their high specific strength compared to conventional structural materials. Recently, the interest in thermoplastic composites have emerged since they can be recycled [1] and are suitable for automation due to their short processing cycles.

Laser-assisted fiber placement (LAFP) with in situ consolidation is an automated manufacturing method for thermoplastic composite structures. During the process, thermoplastic composite tape and substrate are locally melted with a laser heater aimed at the nip point and joined with a compaction roller as shown in Fig. 1. No post-consolidation step is applied in an autoclave, press or oven to give the part its final structure. The process has the potential to reduce material scrap by producing near net-shape parts and decrease energy consumption by eliminating the post-consolidation step.

Achieving in situ consolidation is not straightforward and requires rigorous understanding about the link between the process parameters and the resulting part quality. Several models including tape consolidation [2], intimate contact development [3–5] and void reduction [6] have been used to predict the final geometry and porosity of the laminate. These models require information about the initial state of the tape such as the dimensions, surface profile or void content and then, using the temperature and pressure history of a given process, calculate the micro- and meso-scale changes during manufacturing. This information is usually obtained from the as-received tape.

For conventional composite manufacturing techniques such as autoclave consolidation or press molding, obtaining such parameters from the as-received tapes may not influence the accuracy of the predictions due to comparably slow heating rates (< 20 °C/s) and long dwell times (on the order of minutes). However, during LAFP, heating rates are much higher (up to 2000 °C/s) and no compaction pressure is applied on the tape during heating. Besides, laser heating relies on radiation, whereas the material is heated by conduction/convection during conventional manufacturing techniques. This might lead to a different heat flux and temperature distribution during heating. Moreover, following the heating phase, compaction of the tape and the substrate can only occur during the limited time spent under the compaction roller (< 1 s). This means that any change in the microstructure during the heating phase can be expected to have a more pronounced effect on an in situ consolidated part compared to a conventionally manufactured part. Albeit originally developed for conventional methods, the above-mentioned models have been used to predict the quality of the parts manufactured with LAFP [7–10]. It has been assumed that the properties of the as-received tape does not change during the heating phase of the LAFP process.

* Corresponding author.
E-mail address: ozan.celik@tudelft.nl (O. Çelik).

https://doi.org/10.1016/j.compositesa.2021.106575
Received 1 April 2021; Received in revised form 14 June 2021; Accepted 23 July 2021
Available online 3 August 2021

The negative changes in the micro- and meso-structure of a thermoplastic composite material at high temperature in the absence of pressure are termed as *deconsolidation* [11]. It has been studied mostly for reheating/cooling of pre-consolidated composite laminates, which is typically encountered in applications such as resistance welding [12], induction welding [11] and stamp forming [13]. Four different mechanisms have been identified as the source of deconsolidation of pre-consolidated laminates so far:

- Void growth, motion and coalescence [14–16],
- Decompaction of the fiber–matrix network due to release of residual stresses in the preform [17],
- Thermal expansion and viscoelastic behavior of the resin [18],
- Thermal expansion of dissolved moisture in the resin [13].

Deconsolidation of an individual layer of CF/PEEK prepreg material was investigated in the recent works of Slange et al. [13] and Krämer et al. [19]. In the work of Slange et al. [13], three different initial conditions were studied: as-received prepreg plies, plies which were annealed below the melting temperature for 3 h and plies that were press-consolidated above the melting temperature for 20 min. The same deconsolidation treatment was applied on these specimens by reheating them in an oven at 390 °C for 1 h. The as-received and annealed plies were significantly affected by the deconsolidation treatment as an increase in surface roughness due to loose dry fibers at the surface and local out-of-plane waviness were observed. On the contrary, press consolidated plies remained intact after the deconsolidation treatment. They hypothesized that the plies deconsolidated due to the residual stresses introduced during the prepreg manufacturing process. Krämer et al. investigated in-plane waviness formation for single-ply 300 × 300 mm^2 CF/PEEK sheets during heating on a hot plate under vacuum [19]. It was shown that in-plane waviness formed during cooling between the melting and crystallization temperatures of the polymer. It was discussed that the main contributor to in-plane waviness formation is the compressive stress on the fibers caused by tool-ply interaction. They observed the waviness formation using an optical camera, which does not provide the height information of the tape surface. Therefore, out-of-plane waviness, which is more relevant to inter-ply porosity in the final laminate than in-plane waviness, was not quantified and its formation was not discussed. Moreover, these studies were performed under conditions similar to hot press or oven processing, leading to low heating rates as previously mentioned.

While a substantial amount of work has been done on characterizing the deconsolidation behavior of pre-consolidated laminates under slow heating rates, there is very little research performed on individual layers of tape under rapid laser heating. Kok et al. attempted to capture the deconsolidated state of the tape by reducing the compaction pressure applied by a LAFP machine using shims and placing the tape on a cold tool to freeze the microstructure as soon as possible [20]. Cross-sectional micrographs of the tapes placed with reduced pressure suggested that the heated surface of the CF/PEEK prepreg tape is rougher and has more dry fibers compared to the pristine tape. In a follow-up study, they quantified the through-thickness fiber, resin and void content in the cross-sections and concluded that the effects of deconsolidation can be observed up to 20 μm from the heated tape surface, which corresponds to 15% of the initial tape thickness [21]. Their work highlights the importance of the heating phase of LAFP; however, the measurements were made after the tape was placed on the tool and cooled down. Therefore, there is still a knowledge gap about the state of the tape at the nip point and the evolution of deconsolidation from the beginning of heating until the nip point (denoted in Fig. 1).

Moreover, the experiments in the literature were conducted for a specific set of laser settings and placement speed. Therefore, the effects of different heating conditions remain unresolved. There are studies which claim that increasing the heated length of the tape is beneficial for bonding because the heat soak in the tape prevents rapid cooling under the compaction roller [22,23]. Recent advances in laser heating technology such as Vertical-Cavity Surface-Emitting Lasers (VCSEL) or zoom homogenizers make it possible to adjust the heated length during processing [24]. Also, the response of the material under different placement speeds (leading to different heating times) is of interest since a wide range of placement speeds (100–400 mm/s [25]) have been reported in the literature. To use the full potential of tailoring the heating phase of the LAFP process for different placement speeds, one must discover the extent of deconsolidation and underlying mechanisms for different heated lengths and heating times.

The objective of this paper is therefore to understand how the micro- and meso-structure of the thermoplastic tape is influenced during rapid laser heating, considering different heated lengths and heating times. To do that, a novel experimental setup was designed to measure the temperature and surface profile of the thermoplastic tape *in situ* during heating with a laser heater. Geometric tape properties such as waviness, out-of-plane deformation and arc length width were calculated from in situ profile measurements. Additionally, the surface roughness, void content and thickness were measured ex-situ for additional insight on the deconsolidation mechanisms.

2. Materials and methods

2.1. Experimental setup

The experimental setup designed for creating varying heated lengths and heating times, and measuring the temperature and surface deformation in-situ during laser heating is shown in Fig. 2. The setup comprises an aluminum tool which was designed to hold a piece of composite tape in place. A VCSEL laser heat source was pointed towards the tape with an angle of 45° from the table surface. A thermal camera and a laser line scanner were used to capture the temperature and surface deformation, respectively.

The laser heat source is a TRUMPF PPM411-12–980-24 laser module,

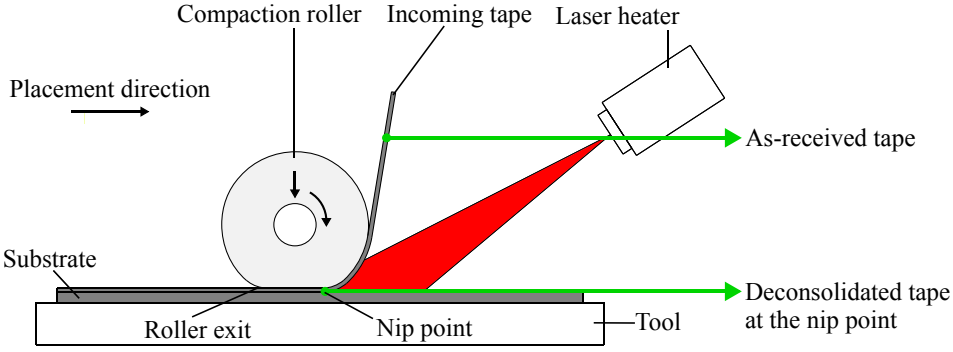

Fig. 1. Typical LAFP process. The as-received and deconsolidated forms of the incoming tape are highlighted.

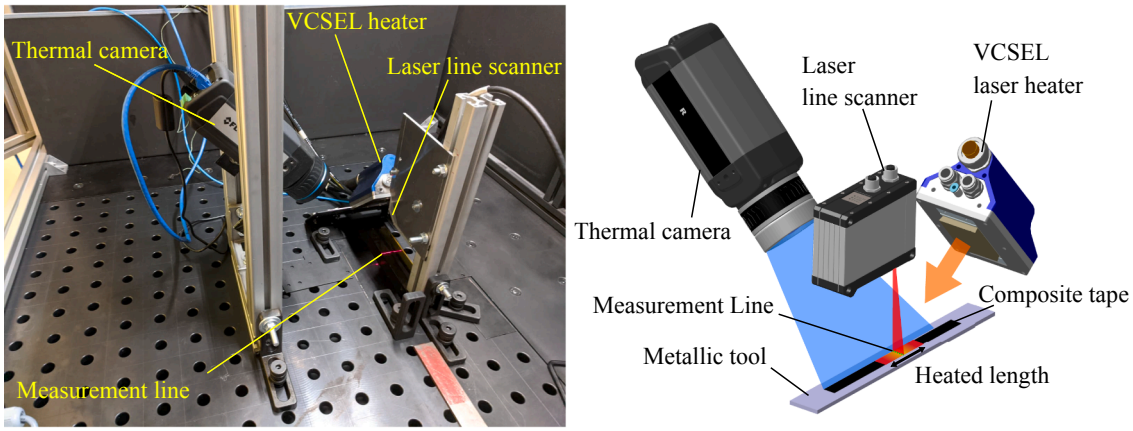

Fig. 2. The experimental setup to measure temperature and surface profile in situ during rapid heating of the composite tape and its schematic description.

with a total output capacity of 2.4 kW. The device contains 12 heating zones which may be independently activated to get a tailored heating profile. The emitted infrared radiation has a wavelength of 980 nm [26]. The independent heating zones of the VCSEL heater were selectively activated and the laser power was adjusted to obtain different heated lengths and heating times.

Temperature on the tape surface during heating was measured in situ with a FLIR A655sc long-wave infrared (LWIR) camera. The detector of the camera has a resolution of 640 × 480 pixels which corresponds to ~ 0.25 mm/pixel in this setup. The thermal images were captured at a sampling rate of 25 Hz. The accuracy of the temperature measurement is ±2 °C or ±2% (whichever is greater). The camera was calibrated in the range of 100–650 °C.

For in situ surface profile measurements, a Micro-Epsilon scanCONTROL 2950–25 laser line scanner (LLS) was used. The sensor operates according to the principle of optical triangulation. First, a laser line is projected onto the target surface via a linear optical system. Then, the diffusely reflected light from the laser line is replicated on a sensor array and evaluated in two dimensions [27]. The tape profile was sampled with 100 Hz during heating. The resolution in the tape thickness direction was 2 μm. The maximum resolution in the tape width direction was ~ 20 μm. The resolution values were reported for ideal conditions. They might be influenced by the reflectivity of the prepreg in melt conditions.

2.2. Tape deconsolidation experiments

The experiments were conducted using TC1200 carbon-fiber reinforced polyether-ether-ketone (CF/PEEK) prepreg tapes produced by Toray Advanced Composites with a fiber volume fraction of 59%. The tapes were in a 12.7 mm (1/2 in.) wide-slit form. Relevant physical properties supplied by the manufacturer and geometric properties measured from cross-sectional images of the as-received tape are given in Table 1. For each experiment, a 100 mm-long prepreg tape sample was positioned on the tool surface and fixed with Kapton tapes at the edges.

Table 1
Measured geometric properties of the as-received CF/PEEK tape along with physical properties provided by the manufacturer. The values in parentheses show the standard deviation for the measured properties.

Glass transition temperature (T_g) [50] (°C)	Melting temperature (T_m) [50] (°C)	Thickness (μm)	Width (μm)	Volumetric void content (%)	RMS surface roughness (μm)
143	343	151.34 (7.7)	12627 (50)	0.71 (0.10)	1.69 (0.39)

Two heated lengths, namely 30 mm and 80 mm, were examined. These values represent the lower and higher extreme cases for most of the heated lengths reported in the literature (e.g., 30 mm [28], 52 mm [22], 60 mm [29]). The experiments were performed with two different heating times, namely 0.2 s and 0.8 s. The heating time was bounded on the lower end with the available laser power to heat the material to a temperature above the melting temperature. The high heating time was determined so that the maximum temperature was reached in a similar manner to a rather slow placement speed in the actual LAFP process (37.5 mm/s, calculated for the heated length of 30 mm). The target temperature on the tape at the measurement area for each heated length and heating time was 360 °C. However, due to deformation of the tape at increased temperatures, a range between 340–400 °C was observed. This choice was made based on the achievable temperature above the melting point of the material with the shortest heated length and heating time.

To obtain the variations in the heated length, different zones on the VCSEL heater were activated. To reach the target temperature at the predefined heating time, the power level at each heating zone was adjusted. Table 2 provides the laser settings used in the experiments. Four samples were tested at each laser setting.

2.3. In-situ measurements

The surface profile and temperature along the width of the tape were measured at the center of the prepreg tape in the length direction ("Measurement Line" in Fig. 2) during laser heating. The aim of the in situ measurements was to understand the changes between the as-received tape and the deconsolidated tape at the nip point during the actual LAFP process (please refer to Fig. 1). The measurements before heating represented the as-received tape, whereas the measurements just after heating represented the deconsolidated tape at the nip point.

It should be noted that some assumptions are inherent when the state of the tape at the end of heating in the tape deconsolidation experiments is accepted as the state at the nip point in an actual LAFP process. Firstly, the reflection of the laser beams from the substrate on the tape are not considered. The tape is illuminated by only the laser heater and no secondary reflections are present in the experimental setup. Secondly, the cooling of the tape in the shadow prior to the nip point was neglected. The time spent in the shadow is highly dependent on the shape of the compaction roller and placement speed, and varies between a few to tens of milliseconds [8]. Finally, the tapes were heated in a static setup aiming increased control over the heating parameters and collection of high quality data, whereas the tape is heated dynamically during the LAFP process. The incoming tape passes through the laser illuminated zone with the prescribed placement speed, as shown in

Table 2
Laser settings used in the experiments.

Experiment	Heated length (mm)	Heating time (s)	VCSEL zones activated	Power in each zone (%)	Total input power (W)	Equivalent LAFP placement speed (mm/s)
1	30	0.2	7–9	100	600	150
2	30	0.8	7–9	37	222	37.5
3	80	0.2	1–11	90	1980	400
4	80	0.8	1–11	30	660	100

Fig. 1. This might lead to a different through-thickness temperature gradient and influence the laser-affected zone in the thickness direction.

2.3.1. Surface profile

To compare the as-received tape and the deconsolidated tape at the nip point, four quantities were calculated from the surface profile measurements at the end of heating: the maximum out-of-plane (OP) deformation, the wavelength/maximum amplitude of the waviness curves and the width of the tape. The maximum OP deformation was calculated by subtracting the average height of the initial tape from the highest peak of the profile at the end of the heating phase. The waviness curves were obtained by applying a Gaussian filter [30] with a cut-off wavelength of 0.8 mm to the raw data according to the ISO 4288 standard [31]. An example is demonstrated in Fig. 3. In the waviness curves, the vertical and horizontal distances between the maximum peak and the minimum valley were termed as the maximum amplitude (A) and the half wavelength ($\lambda/2$). It was observed that due to warpage of the tape during heating, the projected width was not representative of the actual width of the tape. Hence, the captured surface profile was used to obtain the arc-length width of the specimens, which is also shown in Fig. 3.

To observe the changes in the tape *during* the heating process, time-dependent data was also analyzed. The OP deformation during heating was calculated as the height difference between the tape profile at the analyzed time step and the initial tape profile, normalized by dividing with the initial tape thickness of 0.15 mm. This data was used for qualitative purposes only since abnormal spikes were observed in the surface profiles of a significant amount of specimens. The cause for this is thought to be the reflection of the laser beams emitted from VCSEL heater on the deforming tape surface. It is believed that some of the reflected beams were captured by the LLS, causing irregularities in the surface profile measurement during heating. As soon as the laser heating ended, such disturbances disappeared.

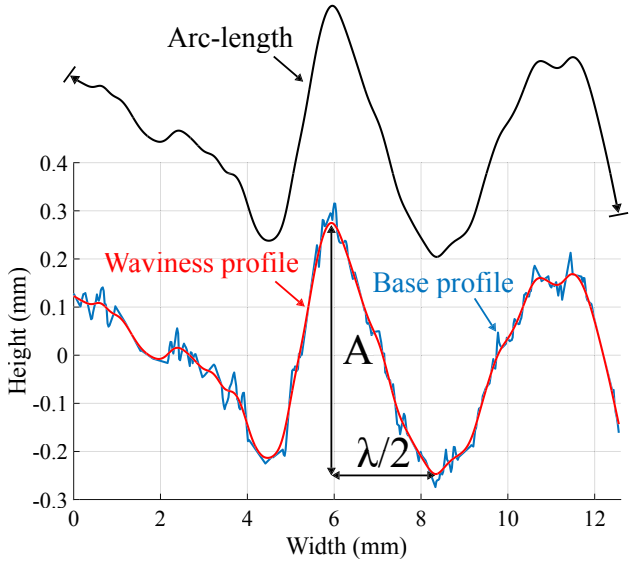

Fig. 3. An example profile obtained from LLS and the corresponding waviness curve. The maximum amplitude (A), the associated half-wavelength ($\lambda/2$) and the arc-length width of the tape are demonstrated.

2.3.2. Temperature

Temperature during heating was extracted from measurement lines placed perpendicular to the fiber direction of the tape as shown in Fig. 5 for each specimen. The location of the measurement lines was determined such that they cover the whole tape width and overlap with the projection of the laser beams emitted from the laser line scanner on the tape (shown in Fig. 2). The emissivity of the tape was calibrated according to the ASTM E1933 standard [32] and found to be 0.84.

Temperature history and time-dependent surface profile data were synchronized after the experiments were completed. LLS measurements were converted to Comma Separated Value (.csv) files using the ScanCONTROL 3D software. The temperature measurements were exported in Matlab-formatted data format (.mat) using the ResearchIR software. Both sets of data were imported to Matlab software and arranged in two separate matrices so that each row shows the surface profile and temperature at a given frame. The surface profile data was cropped manually so that only the tape surface is included. This procedure was not required for the temperature profiles, as the measurement line was already defined to cover the tape width only, as shown in Fig. 5. The final step of the synchronization was the time-wise alignment of both sets of data. The frame at which the heating started was used to align both datasets. This was manually found in the temperature data based on the increase in temperature on the measurement line. In the surface profile data, the beginning of heating was marked by reflections on the tool surface as shown in Fig. 4.

2.4. Ex-situ measurements

Ex-situ surface roughness, void content and thickness measurements were used to explain deconsolidation mechanisms in more detail with a resolution that could not be achieved during the in situ measurements. These measurements were performed after the tape cooled down to room temperature; therefore, they may not fully represent the state of the tape at the nip point.

2.4.1. Surface roughness

An Olympus OLS 3100 laser scanning confocal microscope (LSCM) was used to measure the local surface roughness. Due to the limitations of the equipment, four confocal images were captured for each specimen at 20%, 40%, 60% and 80% of the tape width. These images were captured at 20× magnification, which corresponds to an area of 640 μm (along the fiber direction) × 480 μm (transverse to the fiber direction). From these measurements, ten line surface profiles were extracted along the direction transverse to the fibers. Following the guidelines in the ISO 4288 standard [31], a high-pass filter of 96 μm was applied to each primary line profile obtained for an evaluation length of 480 μm (transverse to fiber direction) to separate roughness profile from the primary profile and remove any global curvature effects. The average root-mean-square (RMS) roughness of each image were calculated by averaging the RMS roughness of ten surface profiles. Finally, the mean RMS roughness was calculated for each specimen by averaging the RMS roughness at 20%, 40%, 60% and 80% of the tape width.

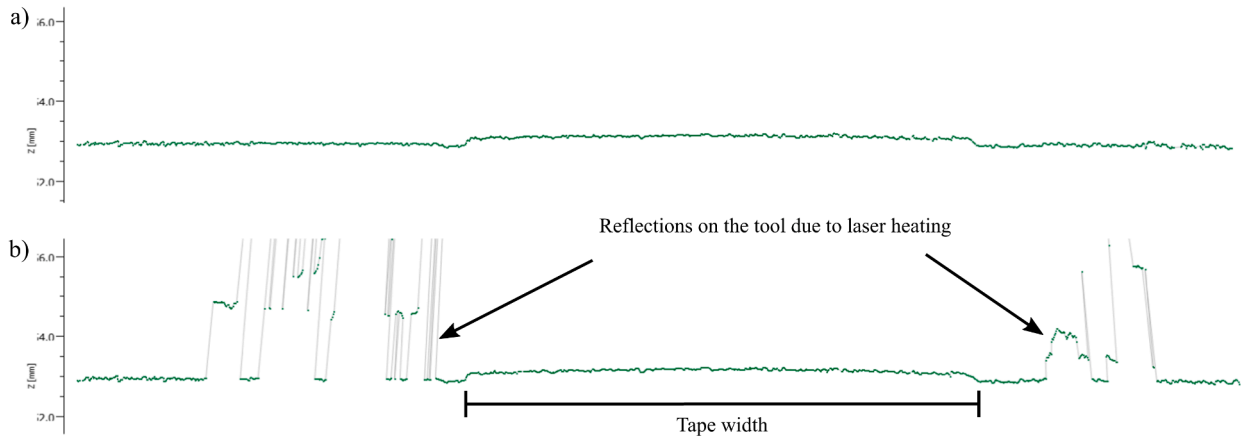

Fig. 4. Example of the surface profile of the tape and the tool a) before heating, b) at the moment heating started.

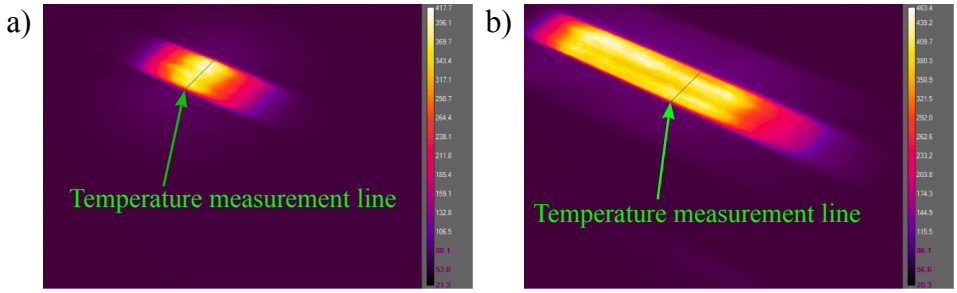

Fig. 5. Representative thermal images of samples heated with heated lengths of a) 30 mm b) 80 mm.

2.4.2. Void content and thickness

The final void content and thickness of the composite tape were determined by cross-sectional microscopy. To prepare the cross-sectional microscopy samples, the specimens were cut with an offset of 3 mm in the fiber direction from the measurement line shown in Fig. 2 to account for material removal during polishing and grinding. The specimens were then embedded into slow-curing mounting epoxy (Struers Epofix) and ground/polished in a Struers Tegramin-20 specimen preparation equipment. A Keyence VHX-2000 digital microscope was used to capture the cross-sectional images.

The final void content of the samples was determined using the native image analysis software of the microscope (VHX-2000 Communication Software). The voids were separated from the fibers and resin using a gray level threshold analysis, similar to the segmentation method proposed in the authors' previous work [33]. To compare the specimens heated with different laser settings, the global void content along the complete width of the tape was determined.

The final tape thickness was measured from the perpendicular distance between the top and bottom surfaces of the tapes. Similar to the void content, it was observed that the thickness at locations corresponding to the peak of the waviness curve of the surface profile was locally high. Hence, the thickness was measured at 20%, 40%, 60% and 80% of the width of the tape. Three measurements were made and averaged at each location.

2.5. Analysis of Variance (ANOVA)

Two-way ANOVA method was applied on the results of the in situ and ex-situ measurements to assess the effects of the heated length and heating time quantitatively. The Matlab built-in function *anovan* was used for this purpose [34]. The outputs of this function were p-values for laser settings shown in Table 2. p-values smaller than 0.05 imply that the mean response of the specific setting is different from the mean of all data within a confidence interval of 95%. The effect of such a parameter can be considered statistically significant.

3. Results

3.1. Waviness at the nip point

Representative tape profiles before and after heating for each process variable are shown in Fig. 7. The profiles after heating were captured at the end of laser heating without any further cooling so that they represent the state of the tape at the nip point in an actual LAFP process under the assumptions explained in Section 2.3. It can be observed that laser heating caused significant changes in the waviness of the tape in the width direction for all heating parameters. To explain the differences qualitatively, the classification scheme based on the number and distribution of waves which was proposed in the work of Thor et al. [35] can be used. In [35], two kinds of waviness are defined for distributed waves: in-phase distributed (with constant amplitude and wavelength) and stochastically distributed (with varying amplitude and wavelength) waviness. The heated length had an effect on the shape of the waviness after heating. The samples with a heated length of 80 mm (Fig. 7b, d) resulted in in-phase distributed waviness. However, the samples with a heated length of 30 mm (Fig. 7a, c) showed stochastically distributed waviness. Heating time did not seem to affect the shape of the waviness at the end of heating.

A quantitative assessment of the effect of laser heating on the waviness can be made with the resulting maximum amplitude (A) and wavelength (λ) values presented in Table 3. Assuming that the as-received tape is almost perfectly flat ($A = 0$ and $\lambda = \infty$), the laser heating process increased A and decreased λ. The maximum amplitude at the nip point state ranged between 0.21 mm (30 mm heated length, 0.8 s heating time) and 0.62 mm (80 mm heated length, 0.2 s heating time). The associated wavelength ranged between 4.24 mm (30 mm

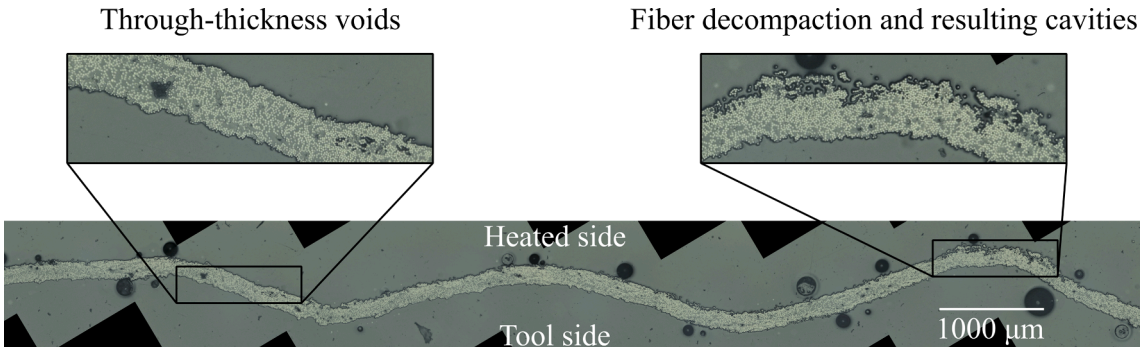

Fig. 6. Representative cross-sectional image of a deconsolidated tape.

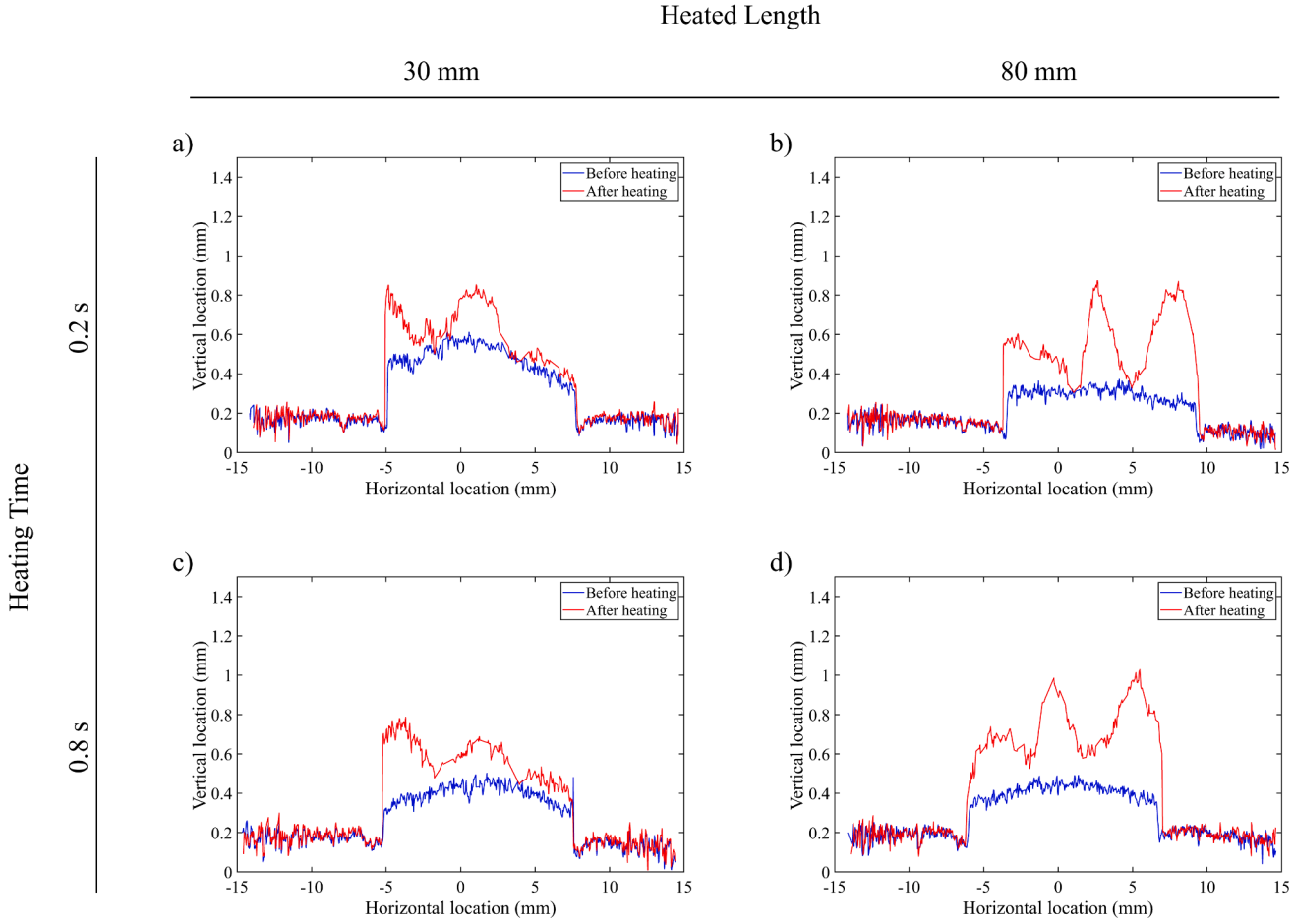

Fig. 7. Representative surface profiles before and after heating for a) 30 mm heated length and 0.2 s heating time, b) 80 mm heated length and 0.2 s heating time, c) 30 mm heated length and 0.8 s heating time, d) 80 mm heated length and 0.8 s heating time.

Table 3
Process parameters and *in situ* measurements immediately after the end of laser heating (nip point state). The values in parentheses show the standard deviation of the means of all experiments. Ideal as-received tape data is added for ease of comparison.

Heated length (mm)	Heating time (s)	Max. amplitude (A) (mm)	Wavelength (λ) (mm)	Max. OP deformation (mm)	Arc-length width change (%)
Ideal as-received tape		0	∞	0	0
30	0.2	0.25 (0.07)	4.24 (1.86)	0.48 (0.03)	2.5 (0.3)
30	0.8	0.21 (0.10)	4.89 (1.55)	0.40 (0.02)	1.4 (0.3)
80	0.2	0.62 (0.15)	5.24 (1.41)	0.64 (0.16)	5.5 (0.2)
80	0.8	0.54 (0.16)	4.70 (1.40)	0.70 (0.09)	3.9 (0.7)

heated length, 0.2 s heating time) and 5.24 mm (80 mm heated length, 0.2 s heating time).

The heated length and the heating time had adverse effects on the maximum amplitude. Increasing the heated length from 30 mm to 80 mm caused an increase of 0.37 mm (148%) and 0.33 mm (157%) in the maximum amplitude for the heating times of 0.2 s and 0.8 s, respectively. Increasing the heating time from 0.2 s to 0.8 s resulted in a decrease of 0.04 mm (16%) and 0.08 mm (13%) in the maximum amplitude for the heated lengths of 30 mm and 80 mm, respectively. A clear trend was not observed for the wavelength for neither of the heating parameters. The effects of the heating time and heated length can be further analyzed using the results of ANOVA shown in Table 5. The heated length had a statistically significant effect on A ($p = 0.0001$) but not on λ ($p = 0.3711$). The heating time did not have a significant effect on neither A nor λ ($p = 0.335$ and $p = 0.8048$, respectively). This confirms the qualitative assessment on the effect of the heating time on the waviness shape.

3.2. Temperature history and out-of-plane deformation

Fig. 8a and Fig. 8b show representative synchronized temperature and OP deformation plots along the width of the tape at the measurement line (referring to Fig. 2) for different heated lengths (30 and 80 mm). The measurements are presented from the beginning until the end of the heating. The first interesting observation was that the temperature during heating was not uniform although the VCSEL laser heater provides a nearly homogeneous irradiance in the width direction [36]. In the beginning of the heating process, the temperature variation along the width of tape specimens was ~ 0.8%. However, as the temperature exceeded T_g (at 150–200 ms from the beginning of heating), temperature variation started increasing. By the time some parts of the tape exceeded T_m (at 500–800 ms from the beginning of heating), temperature variations of up to 50% were observed along the width.

Comparison of the temperature and the deformation history of the tape yielded further interesting results. At the moment the temperature exceeded T_g over the width, a sudden increase in the deformation was observed. Afterwards, the material deformed steadily until T_m was reached. At 500–800 ms (depending on the location in the width direction), T_m was reached and the material deformed drastically, causing significant waviness in the tape. It can be seen that the high and low values in the temperature plots followed a similar trend with the peaks and valleys in the deformation plots, respectively.

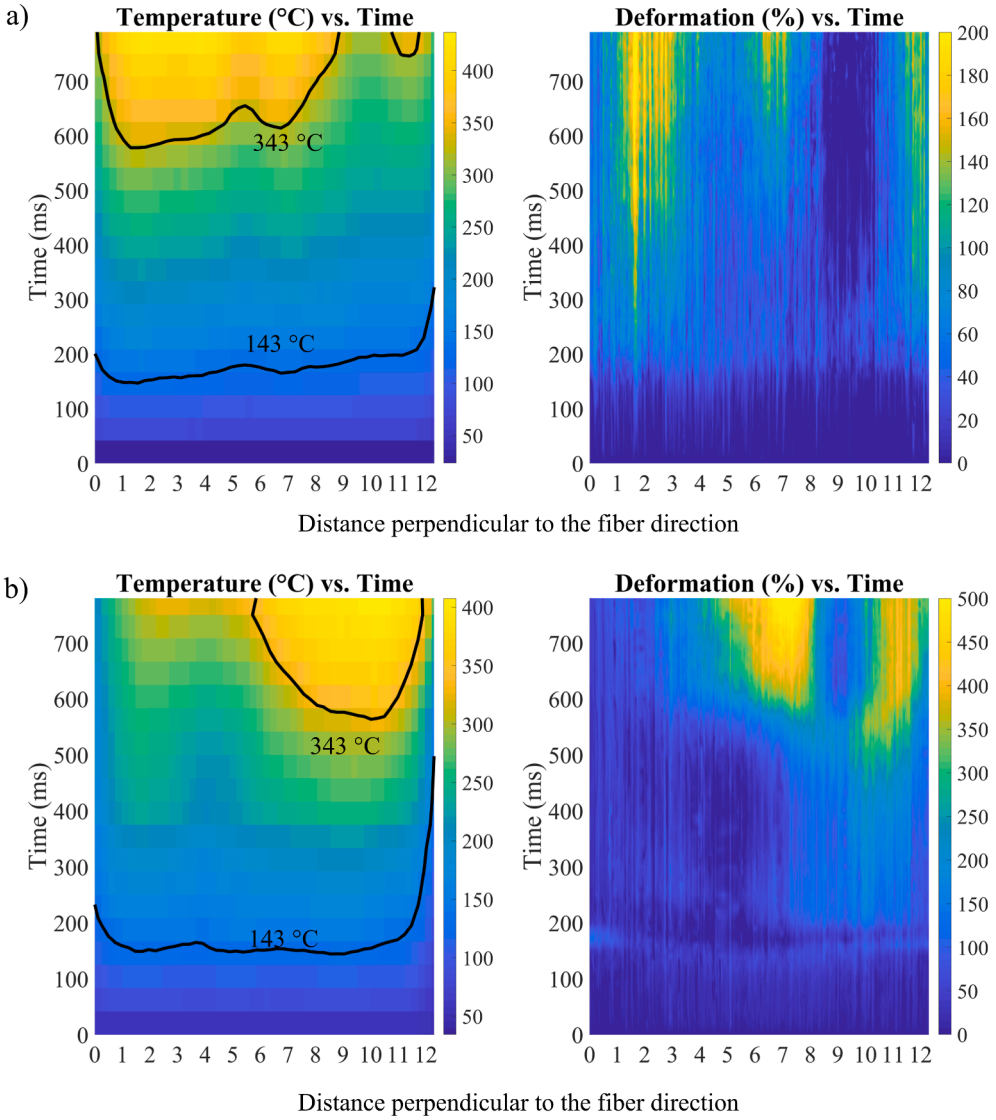

Fig. 8. Representative synchronized temperature and out of plane deformation plots at the measurement line. The data is from experiments with long heating time (0.8 s) and a) small heated length (30 mm), b) large heated length (80 mm). The moments when T_m (343 °C) and T_g (143 °C) of PEEK are reached are marked on the temperature plots. The difference in the scales of the deformation plots is to be noted.

The maximum OP deformation at the nip point for different heating parameters is shown in Table 3. Laser heating caused OP deformation for all cases. The maximum OP deformation at the nip point state ranged between 0.40 mm (30 mm heated length, 0.8 s heating time) and 0.70 mm (80 mm heated length, 0.8 s heating time). Increasing the heated length from 30 mm to 80 mm resulted in an increase of 0.16 mm (33%) and 0.30 mm (75%) in the maximum OP deformation for the heating times of 0.2 s and 0.8 s, respectively. A clear trend was not observed for the effect of the heating time on the maximum OP deformation. Statistical significance of the effects of the heating time and heated length on maximum OP deformation are assessed in Table 5. ANOVA indicated that the effect of heated length was statistically significant ($p = 0.012$) whereas the effect of heating time was statistically insignificant ($p = 0.7885$). The effect of the heated length can also be observed from the deformation plots in Fig. 8. The tape heated with the 30 mm heated length (Fig. 8a) deformed much less than the tape heated with the 80 mm heated length (Fig. 8b).

3.3. Arc-length width at the nip point

Table 3 shows the change in the arc-length width of the tape at the nip point state. Laser heating increased the arc-length width of the tape between 1.4% (30 mm heated length, 0.8 s heating time) and 5.5% (80 mm heated length, 0.2 s heating time) of the arc-length width of the tape before heating. The arc-length width increased more as the heated length was increased from 30 mm to 80 mm (120% and 179% for the heating times of 0.2 and 0.8 s, respectively.) or the heating time was decreased from 0.8 s to 0.2 s (21% and 19% for the heated lengths of 30 and 80 mm, respectively.), keeping the other heating parameter fixed. Table 5 statistically demonstrates the effects of heating time and heated length on arc-length width of the tape at the nip point state. Both the heated length ($p = 0.0000$) and the heating time ($p = 0.0002$) had a significant effect on arc-length width increase.

3.4. Ex-situ measurements

Fig. 6 shows a typical cross-section of a deconsolidated specimen after cooling to room temperature. It can be seen that the surface roughness, void content and thickness differed locally along the width of the tape. Table 4 presents the effects of heating time and heated length on surface roughness, thickness increase and void content after the tape cools down to the room temperature. Table 5 shows the results of ANOVA on the influence of the heating parameters on the ex-situ measurements.

Laser heating led to an increase in the RMS surface roughness for all heating times and heated lengths. The lowest RMS roughness was observed for 30 mm heated length and 0.2 s heating time (252% increase). The highest RMS roughness was observed for 80 mm heated length and 0.8 s heating time (712% increase). Both heating parameters had a statistically significant effect on the surface roughness according to ANOVA ($p = 0.0000$ and 0.0000 for heated length and heating time, respectively). Also, the interaction term was statistically significant ($p = 0.0000$). Examining the mean values in Table 4, the interaction term implies that increasing the heating time had a much weaker effect on the RMS roughness for the heated length of 30 mm (7% increase) compared to its effect for the heated length of 80 mm (75% increase).

Table 4
Process parameters and *ex-situ* measurements after the tape cooled down to room temperature. The values in parentheses show the standard deviation of the means of all experiments. As-received tape data is added for ease of comparison.

Heated length (mm)	Heating time (s)	Mean RMS roughness (μm)	Thickness increase (μm)	Volumetric void content (%)
As-received tape		1.7 (0.4)	0	0.7 (0.1)
30	0.2	6.0 (0.7)	27.3 (1.3)	3.3 (0.7)
30	0.8	6.4 (0.2)	34.5 (6.3)	4.0 (0.1)
80	0.2	7.9 (0.8)	24.8 (3.2)	3.6 (1.0)
80	0.8	13.8 (0.6)	25.6 (10.0)	4.3 (1.6)

After the heating–cooling cycle, the thickness of the tape increased between 25.6 μm and 34.5 μm (∼ 20%) on average for all parameters. However, neither of the heating parameters had a statistically significant effect ($p = 0.2285$ and $p = 0.3824$ for the heated length and heating time, respectively).

All experiments resulted in an increase in void content, whose final values ranges between 3.3–4.3% on average. However, the effects of neither of the heating parameters on the final void content ($p = 0.7043$ and $p = 0.3406$ for the heated length and heating time, respectively) were statistically significant.

4. Discussion

4.1. Deconsolidation mechanisms during rapid laser heating

The results of this research indicate that thermoplastic tapes deconsolidate significantly under laser heating parameters relevant to the LAFP process. Deconsolidation occurred in the form of increased out-of-plane deformation, waviness, arc-length width, roughness, thickness and volumetric void content as shown in Table 3 and 4. The observations and literature point out to the fact that a complex and intertwined relationship is present between the deconsolidation mechanisms and forms of deconsolidation at the micro- and meso-scale. An overall picture of this relationship is shown in Fig. 9. Given the initial tape microstructure and laser heating parameters such as the heated length and heating time (shown with the brown circle), several deconsolidation mechanisms (red rectangles) will be triggered and result in different forms of deconsolidation (blue ellipses). Since the laser heating is affected by the surface properties of the tape, surface roughness and waviness formation lead to non-uniform temperature at the surface (green rounded rectangle), which exacerbates the deconsolidation mechanisms at several locations on the tape. This creates a unique link between the forms of deconsolidation and deconsolidation mechanisms, forming the loop in Fig. 9.

4.1.1. Fiber decompaction

The first of these phenomena is fiber decompaction, which is demonstrated in Fig. 6. It can be observed that fibers do not decompact uniformly along the width of the tape. This can be explained by the local fiber volume fraction near the surface of the as-received tape and softening of the surrounding resin above the glass transition temperature. It has been demonstrated that the incident laser energy on a thermoplastic tape is primarily absorbed by the fibers, as PEEK is practically transparent to laser sources in the wavelength range of 500–2000 nm [37]. The heat is then dissipated to the resin via conduction. The storage modulus of PEEK decreases more than ten-fold above the glass transition temperature [38,39]. This allows the fibers at the surface to move due to the micro-scale residual stresses introduced during tape manufacturing. During the heating experiments, fibers on the surface are thought to absorb the laser energy locally at the areas with a high local fiber volume fraction, soften the resin in their immediate vicinity and decompact.

Fiber decompaction contributed to three forms of deconsolidation: thickness increase, surface roughness increase and final void content. Thickness increase is an obvious outcome of fiber decompaction, as the fibers move in the out-of plane direction. Decompacted fibers increase the surface roughness as well, as there is a correlation between the thickness of the layer with dry fibers at the surface and surface roughness [21]. Moreover, there is an interesting relationship between the fiber decompaction and final void content. Fig. 6 shows that not all the voids are within the tape but some are close to the tape surface where fiber decompaction can be observed. Therefore, it can be concluded that the cavities formed by the motion of fiber bundles at the surface also

Table 5
Results of ANOVA. Values in bold text show that the change in the parameter results in statistically significant changes in the response variable or the interaction between the effect of the parameters is statistically significant ($p < 0.05$).

Process parameter	Max. amplitude (A)	Wavelength (λ)	Max. OP deformation	Arc-length width increase (%)	Max. RMS roughness	Thickness increase	Volumetric void content
Heated length	**0.0001**	0.6138	**0.0012**	**0.0000**	**0.0000**	0.2285	0.7043
Heating time	0.3711	0.9415	0.7885	**0.0002**	**0.0000**	0.3824	0.3406
Interaction	0.8060	0.4649	0.2347	0.3112	**0.0000**	0.4787	0.9452

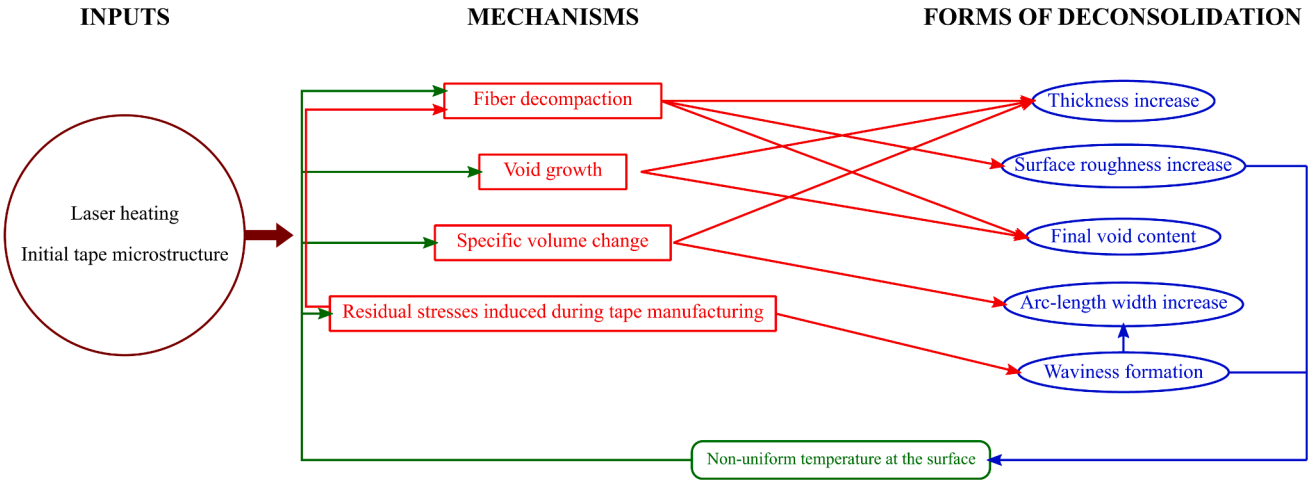

Fig. 9. Deconsolidation mechanisms and the measured forms of deconsolidation during rapid laser heating.

play a major role in void formation during rapid laser heating. A similar phenomenon has already been observed during the re-heating of pre-consolidated composite laminates [14].

4.1.2. Void growth

Void growth is a source of thickness increase of the tape at the nip point. It also determines the final void content in combination with the void formation due to fiber decompaction. The upper bound for void growth due to thermal expansion of air can be calculated by the ideal gas law if the elastic modulus and surface tension of the polymer melt are neglected [14]:

$$V_g(T) = \left(\frac{p_g^0}{p_0}\right)\left(\frac{T}{T_0}\right)V_g^0 \tag{1}$$

where V_g^0, T_0 and p_g^0 are the initial average void volume, temperature and pressure,respectively. p_0 is the atmospheric pressure. Assuming $T_0 = 293$ K (20 °C), $T = 633$ K (360 °C) and $p_g^0 = p_0$, Eq. (1) yields

$$V_g = 2.16V_g^0 \tag{2}$$

Given an initial void content of 0.71% (Table 1), this results in a void content of ~ 1.5% if the volume of the tape is assumed to stay constant (which is another conservative assumption since the volume of the whole tape also increases during heating, which would lead to a lower volumetric void percentage). This value is significantly lower than the final void content of the deconsolidated tapes given in Table 4 (3–4%), meaning that other sources of void formation must take part. It was recently shown that dissolved moisture is not a major source of deconsolidation for blanks manufactured with LAFP [13]. Voids due to fiber traction are thought to be the source of the remaining final void content.

4.1.3. Specific volume change

During laser heating, the increasing specific volume of PEEK contributes to thickness and arc-length width increase. Fig. 10 shows the temperature dependent specific volume of PEEK under ambient pressure, reproduced from the work of Zoller et al. [40]. The specific volume of PEEK at room temperature is 0.764 cm^3/g. Below T_g, the specific volume increases linearly with a rate of 1.2×10^{-4} $cm^3/g°C$. Between T_g and T_m, the specific volume increases in a linear fashion up to 320 °C with a rate higher than the rate below T_g (3.5×10^{-4} $cm^3/g°C$). However, as the temperature approaches T_m, a sudden increase is observed in the specific volume, which can be explained by melting of the crystalline phase of the polymer. Above T_m, the specific volume increases linearly with a rate of 6.1×10^{-4} $cm^3/g°C$. From a qualitative perspective, this behavior resembles with the OP deformation patterns demonstrated in Fig. 8: a steady increase past the T_g and a sharp increase as the temperature approaches T_m is common for both the OP deformation and specific volume of PEEK.

The importance of the specific volume increase of PEEK for tape deformation can be assessed by the theoretical volume increase.

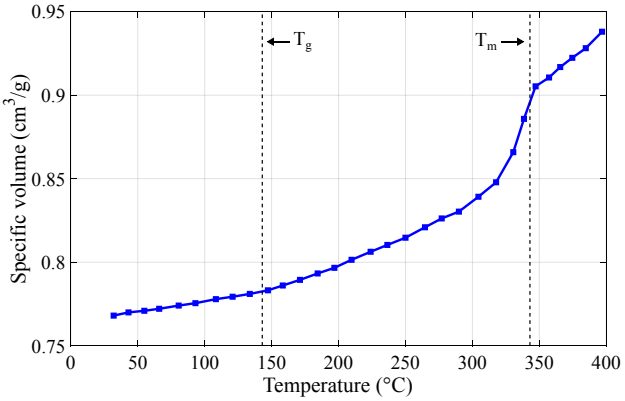

Fig. 10. Temperature dependent specific volume of PEEK at ambient pressure, obtained from isothermal measurements at each temperature. Reproduced from Zoller et al. [40].

According to Fig. 10, the specific volume of PEEK increases by 17.2% at T_m. Assuming that the change of the volume of the carbon fibers is negligible, an equivalent volume increase of 7% is expected for a tape with a resin volume ratio of 41%. The boundary between the solid and molten parts of the tape restricts the movement of PEEK in the longitudinal direction of the tape; so the specific volume change is expected to increase the width and thickness of the tape in the cross-sectional plane perpendicular to the fiber direction. Therefore, the changes in the cross-sectional area of the tape can be used to estimate the volume change. Using the thickness increase from Table 4 and arc-width length increase from Table 3, it can be calculated that the volume change of the tape is between 21–24%. The comparison of the theoretical estimation and experimental data shows that the specific volume increase of PEEK plays a significant role in the deformation of the tape but there should also be other factors which contribute to tape deformation. This confirms the role of fiber decompaction and void growth in the increase in thickness and hence in volume.

4.1.4. Thermal expansion

The thermal expansion in the transverse directions of the tape is relevant for two forms of deconsolidation: arc-length width and thickness increase. Typical CTE values for the CF/PEEK tape and its constituents are given in Table 6. At all temperature levels, the longitudinal CTE of the tape is dominated by the fibers (which have a very small CTE in the longitudinal direction) and the tape can be treated as inextensible in this direction. However, it can be seen that the CTE of PEEK changes drastically as the tape is heated and this is reflected in the transverse CTE of the tape. Therefore, an expansion in the transverse directions can be expected.

Above the melting temperature, the initial tape width of $\sim$ 12.6 mm (Table 1) and transverse CTE of 85 $\times$ 10^{-6} /°C (Table 6) results in a width increase of 1 μm. In the thickness direction, a sub-micron increase is expected due to thermal expansion since the initial thickness is 0.15 mm. These values are negligible compared to the order of magnitude of the deformations in the tape. Therefore, it can be stated that thermal expansion does not play a significant role in deconsolidation of the thermoplastic tapes slit in narrow widths and it was excluded from the mechanisms in Fig. 9.

4.1.5. Residual stresses induced during tape manufacturing

The release of residual stresses in the thermoplastic tape is relevant to two forms of deconsolidation: increased surface roughness due to fiber decompaction in the micro-scale and waviness formation in the meso-scale. These stresses are introduced to the thermoplastic tape during the production process when individual fibers or fiber bundles are stretched, compressed or bent, and subsequently locked upon the solidification of the resin [13]. When the surface of the material reaches T_g, only individual fibers can decompact at the surface since the majority of the resin is in solid state beneath the tape surface. This leads to deformations at the scale of a fraction of the initial thickness of the tape as shown in Fig. 8. However, when more resin content softens as the heating continues, motion of larger fiber bundles are enabled. This results in deformations in the order of multiple initial tape thicknesses in the out-of-plane direction, which cannot be explained by other mechanisms of deconsolidation discussed in the previous sections.

Table 6
Typical coefficients of thermal expansion (10^{-6}/°C) of CF/PEEK and its constituents.

Material	Below T_g	Between T_g and T_m	Above T_m
CF–longitudinal	−1.2 – −0.5[a] [51,52]	0.5[a] [52]	1.1[a] [52]
CF–transverse	4.0[a] – 12.0 [51,52]	5.5[a] [52]	6.8[a] [52]
PEEK	50.0 – 70.0 [53,54]	Increases up to 250 [54]	No data available
CF/PEEK–longitudinal	0.4 [55]	0.0[b] [55]	0.0[b] [51]
CF/PEEK–transverse	30.0 [55]	80.0[b] [55]	85.0[b] [51]

[a] Calculated using PAN-based HTA 5131 carbon fiber data.
[b] Estimated values.

4.1.6. Non-uniform temperature at the surface

Rapid laser heating is unique in the sense that the forms of deconsolidation and deconsolidation mechanisms are linked to each other via the non-uniform temperature at the surface, as demonstrated in Fig. 9. Therefore, the relationship between tape deformation and non-uniform temperature is very important. Fig. 8 demonstrates that the temperature profile and the deformation of the tape followed similar patterns. Also, T_g and T_m mark important points for the non-uniformity of temperature and deformation of the tape.

The initiation of the temperature non-uniformity can be explained by fiber decompaction, which starts around T_g as a result of the reduction in the storage modulus of the resin. As the decompacted fibers moved closer to the laser source, the local heat flux on them increased. This led to an increase in local temperature and further softening of the resin accompanied with more decompaction of fibers.

While the temperature non-uniformity was initiated by fiber decompaction, it was succeeded by waviness formation. This led to even larger variations in tape temperature due to changing angle of incidence at the peaks and valleys formed on the surface. At the beginning of the heating process up to T_g, the coefficient of variation of the temperature along the width of the specimens was on the order of $\sim$ 1%. This value is similar to the calculations presented in the work of Yan et al. [41]. They claimed that on the surface of a thin composite layer with uniform fiber distribution, temperature variation due to the absorption rate difference between the fibers and resin is 0.5%. However, as the specimen reached T_m during the experiments presented in this paper, the coefficient of variation of the temperature along the width raised up to 50%.

The importance of the unique link between the heating and tape deformation mechanisms becomes clearer when the results in this work are compared with the behavior during hot plate heating of the same CF/PEEK material [19], where heat is transferred via conduction between the hot plate and composite. Contrary to laser heating, waviness formation was reported only in the cooling stage and not in the heating stage during deconsolidation with a hot plate. This shows that the mode of heating plays a significant role and deconsolidation should be investigated specifically for the heating device of interest.

4.2. Relevance to LAFP process

Different forms of deconsolidation affect a number of aspects during the LAFP process. The increase in fiber decompaction induced surface roughness is important for bond strength development at the interface since resin must flow through dry fiber bundles to create effective intimate contact [10]. More dry fibers at the tape surface would hinder effective intimate contact development. The RMS roughness results in Table 4 show that the heating strategies that would result in less dry fibers at the surface are reducing the heated length of the tape or increasing the placement speed provided that the nip point temperature is kept fixed. This observation is positive for the industry, as higher placement speeds are expected to result in less dry fibers at the tape surface at the nip point.

The thickness at the nip point influences void compaction and heat transfer during the LAFP process. Void consolidation models such as the ones from Pitchumani et al. [6] and Simacek et al. [16] use the thickness at the nip point (and the subsequent momentary thickness during compaction) to calculate the pressure distribution within the composite material under the compaction roller. Also, as explained in the previous sections and shown in Fig. 6, void growth and fiber decompaction play an important role in the change in tape thickness. Since these mechanisms are local and are not typically observed at every location along the

tape width, the tape thickness increases non-uniformly at the nip point regardless of the heating strategy. This might cause non-uniform pressure distribution at the tape surfaces which are in contact with the compaction roller and the underlying substrate. The thickness increase and non-uniform contact should be incorporated to tape consolidation models to find the final void content of the fiber placed structures more accurately. The thickness increase at the nip point is also important for the through-thickness temperature distribution as the dominating heat transfer mechanism is internal conduction [24]; therefore, it should be considered in the heat transfer models.

Waviness formation at the nip point has potential consequences on mechanical aspects such as non-uniform pressure distribution under the compaction roller, more entrapped air at the interfaces and deviation of the fiber orientation from the design in the thickness direction of the part. In addition, optical-thermal phenomena may be affected by the waviness at the nip point, as the reflection of the laser beams in the cavity formed near the nip point is closely linked to the geometry of the tape and substrate surfaces [37,42]. This would eventually affect the temperature distribution and increase the non-uniformity along the width. The heated length is the predominant factor for the maximum amplitude of the waviness at the nip point as shown in Table 3 and Table 5. This would mean that increasing the heated length of the tape by aiming the laser more towards the tape or activating more emitters would result in more waviness formation. The studies from Grouve et al. [22] and Di Francesco et al. [43] showed that increasing the heated length of the tape led to increased fracture toughness and degree of intimate contact, respectively. This implies that increased waviness during the heating phase may not necessarily affect bond formation. The compaction behavior of deconsolidated tapes should be investigated in further detail to completely understand bond strength development during LAFP.

Tape width after placement is an important factor for LAFP due to its effects on gaps/overlaps in the final laminate. It has been traditionally explained with squeeze flow of the tape under the compaction roller [2]. Dimensional changes in the tape during the heating phase have been neglected so far. The experimental results presented in [44] show that a single CF/PEEK tape placed on an 8-layer cross-ply laminate widens by 8–10% for a nip point temperature between 350–400 °C, with little dependency on the applied compaction force. The limited effect of the compaction force on tape widening suggests that the heating phase of the process plays a significant role for the final tape width. The results of this study confirm this hypothesis, as the arc-length width of the tapes increased significantly (up to 5.5%) at the nip point state. When Table 3 is investigated, it can be seen that the arc-length width and the maximum amplitude of the waviness show a correlation (both increase with increasing heated length and decreasing heating time). This implies that the arc-length width can be heavily influenced by the waviness formation, which can also be seen in Fig. 3.

Table 3 showed that the heated length and heating time had a positive and negative correlation with the arc-length width of the tape at the nip point, respectively. An interesting outcome is that the heated length and laser power should be continuously optimized to keep the tape width at the nip point fixed for the applications where the placement speed varies, such as helical tape winding [45]. Besides, to accurately predict the final tape geometry, not only the squeeze flow under the roller but also the tape deformation before consolidation should be calculated. Kok [44] took a step in that direction by proposing a model based on quasi-static tape spreading. However, there is still room for improvement as the effects of tape warpage and heating time were not accounted for.

The results presented in this work point out to important phenomena for the heating phase of LAFP; however, additional aspects should be considered for a complete assessment of the final part quality. Firstly, the effects of laser illumination on the substrate should be investigated, as the effect of laminate thickness on deconsolidation is not known. Also, residual stresses in the substrate due to local heating and compaction might influence the deconsolidation behavior of the substrate. Another factor that might possibly affect the deconsolidation of the incoming tape is the tape tension. In this work, the tapes were fixed to the tool with polyimide films without tension application. Even though the LAFP systems usually run on low tape tension to enable layup of complex geometries [46,47], the effect of tape tension on deconsolidation has not been clearly demonstrated. The authors are investigating this effect in a separate research project. The role of the applied compaction pressure on reducing the effects of deconsolidation has also been identified as a topic for future research. Finally, being out of the scope of this study, residual stress build-up [48] and non-optimum crystallinity levels [49] remain as important challenges to the improvement of the final quality of the in situ consolidated structures.

5. Conclusion

In this study, the effect of rapid laser heating, which is typical to the heating phase of LAFP, on the micro- and meso-structure of the thermoplastic tape was investigated. Thermoplastic tapes were heated with different heated lengths (30 and 80 mm) and heating times (0.2 and 0.8 s) in a dedicated experimental setup. Meso-scale changes in the tape during laser heating were monitored in situ via temperature and surface profile measurements. Surface roughness measurements with a confocal microscope and cross-sectional images taken with an optical microscope were used to gain additional insight into the effects of laser heating at micro-scale.

All of the experiments in this study caused significant changes in the micro- and meso- structure of the tape. These changes are in the form of increased out-of-plane deformation, waviness, arc-length width, roughness, thickness and volumetric void content. It was found that heated length was a significant factor for waviness formation, arc-length width and surface roughness. Heating time had a statistically significant influence on the arc-length width and surface roughness, the latter being only for the large heated length.

As revealed in this work, deconsolidation of the tape during laser heating is influenced by a unique phenomenon: the correlation between the temperature distribution on the tape surface and the peaks and valleys of the surface profile. Increased surface roughness and waviness result in non-uniform temperature at the surface due to varying angle of incidence. As a result of non-uniform temperature, deconsolidation is exacerbated locally. It was also proposed that deconsolidation of the tape during laser heating is a result of multiple mechanisms. Fiber decompaction plays a role in thickness and surface roughness increase. It also creates cavities near the tape surface and contributes to the final void content. Thermal expansion of voids is a partial reason for the final void content and thickness increase. Specific volume change causes an increase in the thickness and the arc-length width. Residual stresses induced during tape manufacturing is a source of waviness formation, which is also a significant contributor to the arc-length width increase.

Based on the results, the following conclusions can be derived for the LAFP process. Higher placement speeds are expected to reduce the amount of decompacted fibers at the tape surface at the nip point, which is beneficial for effective intimate contact development. In order to keep the width of the tape at the nip point constant during a process where the placement speed is variable, the heated length and laser power should be continuously optimized. Heating a larger portion of the tape would lead to more waviness formation, which causes non-uniform temperature at the tape surface and may result in non-uniform pressure distribution under the compaction roller. Increased thickness at the nip point should be considered to calculate void compaction and heat transfer during the process accurately. For future work, it is suggested that the effects of the heating phase are further quantified using constitutive models and implemented in numerical models developed for the analysis of the LAFP process.

CRediT authorship contribution statement

Ozan Çelik: Conceptualization, Methodology, Formal analysis, Visualization, Data curation, Writing – original draft, Writing – review & editing. **Abhas Choudhary:** Conceptualization, Methodology, Investigation. **Daniël Peeters:** Conceptualization, Methodology, Writing – review & editing, Resources, Supervision. **Julie Teuwen:** Conceptualization, Methodology, Writing – review & editing, Resources, Supervision. **Clemens Dransfeld:** Writing – review & editing, Resources, Supervision.

Declaration of Competing Interest

The authors declare that they have no known competing financial interests or personal relationships that could have appeared to influence the work reported in this paper.

Acknowledgments

This work is funded by European Regional Development Fund (ERDF) within the Smart Industry Fieldlab: ACM project under Grant No. KVW-00043.

References

[1] Roux M, Eguémann N, Dransfeld C, Thiébaud F, Perreux D. Thermoplastic carbon fibre-reinforced polymer recycling with electrodynamical fragmentation: From cradle to cradle. J Thermoplast Compos Mater 2017;30(3):381–403. https://doi.org/10.1177/0892705715599431.
[2] Ranganathan S, Advani SG, Lamontia MA. A non-isothermal process model for consolidation and void reduction during in-situ tow placement of thermoplastic composites. J Compos Mater 1995;29:1040–62.
[3] Lee WI, Springer GS. A model of the manufacturing process of thermoplastic matrix composites. J Compos Mater 1987;21(11):1017–55. https://doi.org/10.1177/002199838702101103.
[4] Mantell SC, Springer GS. Manufacturing process models for thermoplastic composites. J Compos Mater 1992;26(16):2348–77. https://doi.org/10.1177/002199839202601602.
[5] Yang F, Pitchumani R. A fractal Cantor set based description of interlaminar contact evolution during thermoplastic composites processing. J Mater Sci 2001;36(19):4661–71. https://doi.org/10.1023/A:1017950215945.
[6] Pitchumani R, Ranganathan S, Don RC, Gillespie JW, Lamontia MA. Analysis of transport phenomena governing interfacial bonding and void dynamics during thermoplastic tow-placement. Int J Heat Mass Transf 1996;39(9):1883–97. https://doi.org/10.1016/0017-9310(95)00271-5.
[7] Levy A, Heider D, Tierney J, Gillespie JW, Lefebure P, Lang D. Simulation and optimization of the thermoplastic Automated Tape Placement (ATP) process. SAMPE 2012;(January). 15p.
[8] Stokes-Griffin CM, Compston P. Investigation of sub-melt temperature bonding of carbon-fibre/PEEK in an automated laser tape placement process. Compos Part A: Appl Sci Manuf 2016;84:17–25. https://doi.org/10.1016/j.compositesa.2015.12.019.
[9] Leon A, Argerich C, Barasinski A, Soccard E, Chinesta F. Effects of material and process parameters on in-situ consolidation. Int J Mater Form 2019;12(4):491–503. https://doi.org/10.1007/s12289-018-1430-7.
[10] Çelik O, Peeters D, Dransfeld C, Teuwen J. Intimate contact development during laser assisted fiber placement: Microstructure and effect of process parameters. Compos Part A: Appl Sci Manuf 2020:134. https://doi.org/10.1016/j.compositesa.2020.105888.
[11] Henninger F, Ye L, Friedrich K. Deconsolidation behaviour of glass fibre-polyamide 12 composite sheet material during post-processing. Plastics, Rubber Compos Process Appl 1998;27(6):287–92.
[12] Shi H, Villegas IF, Bersee HE. Analysis of void formation in thermoplastic composites during resistance welding. J Thermoplast Compos Mater 2017;30(12):1654–74. https://doi.org/10.1177/0892705716662514. https://journals.sagepub.com/doi/pdf/10.1177/0892705716662514.
[13] Slange TK, Warnet LL, Grouve WJB, Akkerman R. Deconsolidation of C/PEEK blanks: on the role of prepreg, blank manufacturing method and conditioning. Compos Part A: Appl Sci Manuf 2018;113:189–99. https://doi.org/10.1016/j.compositesa.2018.06.034. https://linkinghub.elsevier.com/retrieve/pii/S1359835X18302628.
[14] Ye L, Lu M, Mai YW. Thermal de-consolidation of thermoplastic matrix composites-I. Growth of voids. Compos Sci Technol 2002;62(16):2121–30. https://doi.org/10.1016/S0266-3538(02)00144-6.
[15] Lu M, Ye L, Mai YW. Thermal de-consolidation of thermoplastic matrix composites-II. Migration of voids and re-consolidation. Compos Sci Technol 2004;64(2):191–202. https://doi.org/10.1016/S0266-3538(03)00233-1.
[16] Simacek P, Advani SG, Gruber MB, Jensen B. A non-local void filling model to describe its dynamics during processing thermoplastic composites. Compos Part A: Appl Sci Manuf 2013;46(1):154–65. https://doi.org/10.1016/j.compositesa.2012.10.015.
[17] Wolfrath J, Michaud V, Månson JA. Deconsolidation in glass mat thermoplastic composites: Analysis of the mechanisms. Compos Part A: Appl Sci Manuf 2005;36(12):1608–16. https://doi.org/10.1016/j.compositesa.2005.04.001.
[18] Brzeski M. Experimental and analytical investigation of deconsolidation for fiber reinforced thermoplastic composites. Ph.D. thesis;. Technischen Universität Kaiserslautern; 2014.
[19] Krämer ET, Grouve WJB, Koussios S, Warnet LL, Akkerman R. Real-time observation of waviness formation during C/PEEK consolidation. Compos Part A: Appl Sci Manuf 2020;133:105872. https://doi.org/10.1016/j.compositesa.2020.105872.
[20] Kok T, Grouve WJB, Warnet LL, Akkerman R. Intimate Contact Development in Laser Assisted Fiber Placement. ECCM17 - 17th European Conference on Composite Materials 2016;1(June):26–30.
[21] Kok T, Grouve WJB, Warnet LL, Akkerman R. Quantification of tape deconsolidation during laser assisted fiber placement. In: Automated Composites Manufacturing: Third International Symposium; 2017.
[22] Grouve WJB, Warnet LL, Rietman B, Visser HA, Akkerman R. Optimization of the tape placement process parameters for carbon-PPS composites. Compos Part A: Appl Sci Manuf 2013;50:44–53. https://doi.org/10.1016/j.compositesa.2013.03.003.
[23] Stokes-Griffin CM, Compston P. An inverse model for optimisation of laser heat flux distributions in an automated laser tape placement process for carbon-fibre/PEEK. Compos Part A: Appl Sci Manuf 2016;88:190–7. https://doi.org/10.1016/j.compositesa.2016.05.034.
[24] Weiler T, Emonts M, Wollenburg L, Janssen H. Transient thermal analysis of laser-assisted thermoplastic tape placement at high process speeds by use of analytical solutions. J Thermoplast Compos Mater 2018;31(3):311–38. https://doi.org/10.1177/0892705717697780.
[25] Stokes-Griffin CM, Compston P. The effect of processing temperature and placement rate on the short beam strength of carbon fibre-PEEK manufactured using a laser tape placement process. Compos Part A: Appl Sci Manuf 2015;78:274–83. https://doi.org/10.1016/j.compositesa.2015.08.008.
[26] Philips Photonics GmbH. Laser System with Laser Module PPM412-12-980-24 with Driver Unit PPU104-12 Reference and Installation Manual Version 1.1. Tech. Rep.; 2017.
[27] Micro-Epsilon. Operating Instructions scanCONTROL 29xx. Tech. Rep.; 2018.
[28] Hosseini SM, Baran I, van Drongelen M, Akkerman R. On the temperature evolution during continuous laser-assisted tape winding of multiple C/PEEK layers: The effect of roller deformation. Int J Mater Forming 2020:1–19. https://doi.org/10.1007/s12289-020-01568-7.
[29] Stokes-Griffin CM, Compston P. A combined optical-thermal model for near-infrared laser heating of thermoplastic composites in an automated tape placement process. Compos Part A: Appl Sci Manuf 2015;75:104–15. https://doi.org/10.1016/j.compositesa.2014.08.006.
[30] International Organization for Standardization. ISO 16610-21 Geometrical product specifications (GPS)- Filtration-Part 21: Linear profile filters: Gaussian filters. 2011.
[31] International Organization for Standardization. ISO 4288:1996 Geometrical Product Specifications (GPS) - Surface texture: Profile method - Rules and procedures for the assessment of surface texture. 1996.
[32] ASTM E1933-14 (2014). Standard Practice for Measuring and Compensating for Emissivity Using Infrared Imaging Radiometers. 2014. doi:10.1520/E1933-99AR10.2.
[33] Çelik O, Hosseini SMA, Baran I, Grouve WJB, Akkerman R, Peeters MJ. et al. The influence of inter-laminar thermal contact resistance on the cooling of material during laser assisted fiber placement 2021;145(March). doi:10.1016/j.compositesa.2021.106367.
[34] The MathWorks Inc. MATLAB and Statistics Toolbox Release 2017b. 2017.
[35] Thor M, Sause MGR, Hinterhölzl RM. Mechanisms of Origin and Classification of Out-of-Plane Fiber Waviness in Composite Materials–A Review. J Compos Sci 2020;4(3):130. https://doi.org/10.3390/jcs4030130.
[36] Weiler T. Thermal Skin Effect in Laser-Assisted Tape Placement of Thermoplastic Composites. Ph.D. thesis; 2019.
[37] Stokes-Griffin CM, Compston P. Optical characterisation and modelling for oblique near-infrared laser heating of carbon fibre reinforced thermoplastic composites. Opt Lasers Eng. 2015c;72:1–11. doi:10.1016/j.optlaseng.2015.03.016.
[38] Zheng B, Gao X, Li M, Deng T, Huang Z, Zhou H, et al. Formability and failure mechanisms of woven CF/PEEK composite sheet in solid-state thermoforming. Polymers 2019;11(6). https://doi.org/10.3390/polym11060966.
[39] Yurchenko ME, Huang J, Robisson A, McKinley GH, Hammond PT. Synthesis, mechanical properties and chemical/solvent resistance of crosslinked poly(aryl-ether-ether-ketones) at high temperatures. Polymer 2010;51(9):1914–20. https://doi.org/10.1016/j.polymer.2010.01.056.
[40] Zoller P, Kehl TA, Starkweather Jr HW, Jones GA. The equation of state and heat of fusion of poly(ether ether ketone). J Polym Sci: Part B: Polym Phys 1989;27:993–1007.
[41] Yan H, DuPeng TJGL. Meso-scale simulation of temperature field in composite materials under laser irradiation. In: Ding Y, Feng G, Hoffmann DHH, Cao J, Lu Y, editors. Fourth International Symposium on Laser Interaction with Matter, 10173. International Society for Optics and Photonics; 2017. 101730K.
[42] Hosseini SMA, Schäkel M, Baran I, Janssen H, van Drongelen M, Akkerman R. A new global kinematic-optical-thermal process model for laser-assisted tape

winding with an application to helical-wound pressure vessel. Mater Des. 2020b; 193:108854. doi:10.1016/j.matdes.2020.108854.
[43] Di Francesco M, Giddings PF, Scott M, Goodman E, Dell'Anno G, Potter K. Influence of laser power density on the meso-structure of thermoplastic composite preforms manufactured by Automated Fibre Placement. In: SAMPE Long. Beach 2016;53:1689–99.
[44] Kok T. On the consolidation quality in laser assisted fiber placement: the role of the heating phase. Phd thesis;. University of Twente; 2018. https://doi.org/10.3990/1.9789036546065.
[45] Hosseini SMA, Schäkel M, Baran I, Janssen H, van Drongelen M, Akkerman R. A new global kinematic-optical-thermal process model for laser-assisted tape winding with an application to helical-wound pressure vessel. Mater Des. 2020c; 193. doi: 10.1016/j.matdes.2020.108854.
[46] Lukaszewicz DH, Ward C, Potter KD. The engineering aspects of automated prepreg layup: History, present and future. Compos Part B: Eng 2012;43(3):997–1009. https://doi.org/10.1016/j.compositesb.2011.12.003.
[47] Frketic J, Dickens T, Ramakrishnan S. Automated manufacturing and processing of fiber-reinforced polymer (FRP) composites: An additive review of contemporary and modern techniques for advanced materials manufacturing. Additive Manuf 2017;14:69–86. https://doi.org/10.1016/j.addma.2017.01.003.
[48] Dedieu C, Barasinski A, Chinesta F, Dupillier JM. On the prediction of residual stresses in automated tape placement. Int J Mater Form 2017;10(4):633–40. https://doi.org/10.1007/s12289-016-1307-6.
[49] Comer AJ, Ray D, Obande WO, Jones D, Lyons J, Rosca I, et al. Mechanical characterisation of carbon fibre-PEEK manufactured by laser-assisted automated-tape-placement and autoclave. Compos Part A: Appl Sci Manuf 2015;69:10–20. https://doi.org/10.1016/j.compositesa.2014.10.003.
[50] Composites TA. TenCate Cetex® TC1200 PEEK Resin System Product Data Sheet 2017.
[51] Cogswell FN. Thermoplastic aromatic polymer composites: a study of the structure, processing, and properties of carbon fibre reinforced polyetheretherketone and related materials. Butterworth-Heinemann; 1992. https://doi.org/10.1016/B978-0-7506-1086-5.50002-1.
[52] Pradere C, Sauder C. Transverse and longitudinal coefficient of thermal expansion of carbon fibers at high temperatures (300–2500 K). Carbon 2008;46(14):1874–84. https://doi.org/10.1016/j.carbon.2008.07.035.
[53] Barnes JA, Simms IJ, Farrow GJ, Jackson D, Wostenholm G, Yates B. Thermal expansion behaviour of thermoplastic composite materials. J Thermoplast Compos Mater 1990;3(1):66–80. https://doi.org/10.1177/089270579000300107.
[54] Lu SX, Cebet P. Thermal stability and thermal expansion studies of PEEK and related polyimides. Polymer 1996;37(14):2999–3009.
[55] Cogswell FN. The experience of thermoplastic structural composites during processing. Compos Manuf 1991;2(3–4):208–16. https://doi.org/10.1016/0956-7143(91)90142-4.